Hidden order transition in URu_{2}Si_{2}: Evidence for the emergence of a coherent Anderson lattice from scanning tunneling spectroscopy

Ting Yuan, Jeremy Figgins, and Dirk K. Morr

Phys. Rev. B **86**, 035129 — Published 19 July 2012

DOI: 10.1103/PhysRevB.86.035129

Hidden Order Transition in URu_2Si_2: Evidence for the Emergence of a Coherent Anderson Lattice from Scanning Tunneling Spectroscopy

Ting Yuan, Jeremy Figgins and Dirk K. Morr
Department of Physics, University of Illinois at Chicago, Chicago, IL 60607, USA
(Dated: May 31, 2012)

Using a slave-boson approach, we demonstrate that the differential conductance and quasi-particle interference pattern measured in recent scanning tunneling spectroscopy experiments [A.R. Schmidt *et al.* Nature **465**, 570 (2010); P. Aynajian *et al.*, PNAS **107**, 10383 (2010)] in URu_2Si_2 are consistent with the emergence of a coherent Anderson lattice below the hidden order transition (HOT). Its formation is driven by a significant increase in the quasi-particle lifetime, which could arise from the emergence of a yet unknown order parameter at the HOT.

PACS numbers: 74.55.+v, 75.20.Hr, 71.27.+a, 72.15.Qm

I. INTRODUCTION

Heavy-fermion materials exhibit a plethora of exciting phenomena[1] which are believed to arise from the competition between Kondo screening[2] and antiferromagnetic ordering[3]. One of the most puzzling phenomena arises in the heavy-fermion compound URu_2Si_2 which exhibits an onset of Kondo screening around $T \approx 55$K[4,5], and undergoes a second order phase transition at $T_0 = 17.5$K[4–6] into a state with a still unknown, hidden order parameter (HOP). Currently, an intense debate focuses on the nature of this state[5,7,8]. Important new insight into this question has recently been provided by groundbreaking scanning tunneling spectroscopy (STS) experiments[9,10]. Above the hidden order transition (HOT), the differential conductance, dI/dV, exhibits a characteristic Fano lineshape[11]. In contrast, below T_0, a soft gap opens up in dI/dV[9,10] and a quasi-particle interference (QPI) analysis in Th-doped URu_2Si_2 reveals a band structure similar to that expected in the (heavy Fermi liquid) phase of a screened Kondo lattice[9]. Whether dI/dV is consistent with the observed QPI pattern and with the emergence of a coherent Kondo (or Anderson) lattice, is therefore an important question whose answer will provide crucial insight into the nature of the state below T_0.

In this article, we address this question and demonstrate that the experimentally observed dI/dV[9,10] and QPI pattern[9] below the HOT are consistent with the emergence of a coherent Anderson lattice (CAL) and its electronic band structure. In particular, dI/dV exhibits characteristic signatures of the Anderson lattice band structure[10], such as an asymmetric gap, and a peak inside the gap which arises from the van Hove singularity of the heavy f-electron band. In addition, the temperature evolution of dI/dV[9,10] suggests that the formation of the CAL below the HOT is primarily driven by a strong increase in the lifetime of the heavy quasi-particles. Since the observed second order phase transition at T_0 is not expected to result from the emergence of the CAL, we suggest that it is the yet unknown hidden order parameter that drives the increased quasiparticle coherence, thus leading to the formation of the CAL below the HOT.

II. THEORETICAL FORMALISM

Our starting point for the description of URu_2Si_2 is the slave-boson Anderson Hamiltonian[12–16]. In its conventional form, the slave boson is employed to account for valence fluctuations between unoccupied and singly occupied f-electron sites, resulting in an f-electron occupancy $n_f < 1$. However, as we show below, URu_2Si_2 exhibits valence fluctuations between singly and doubly occupied f-electron sites which leads to $n_f > 1$. In order to describe this case, we employ the particle-hole transformed slave-boson Anderson Hamiltonian, which is given by

$$\mathcal{H} = \sum_{\mathbf{k},\sigma} \varepsilon_{\mathbf{k}} c^\dagger_{\mathbf{k},\sigma} c_{\mathbf{k},\sigma} + \sum_{\mathbf{k},\sigma} E_0 f^\dagger_{\mathbf{k},\sigma} f_{\mathbf{k},\sigma} + V \sum_{\mathbf{r}} \left(f^\dagger_{\mathbf{r},\sigma} b^\dagger_{\mathbf{r}} c_{\mathbf{r},\sigma} + H.c. \right) + \sum_{\mathbf{r},\mathbf{r}'} I_{\mathbf{r},\mathbf{r}'} \mathbf{S}^K_{\mathbf{r}} \cdot \mathbf{S}^K_{\mathbf{r}'} \ . \quad (1)$$

$c^\dagger_{\mathbf{k},\alpha}(f^\dagger_{\mathbf{k},\alpha})$ creates an electron with spin α and momentum $\mathbf{k}$ in the light conduction c-band (heavy f-band), and V is the (bare) hybridization between the c- and f-bands. The two-dimensional (2D) conduction band dispersion $\varepsilon_{\mathbf{k}} = 2t(\cos k_x + \cos k_y) - \mu$ with nearest-neighbor hopping t and chemical potential μ is chosen to reproduce the 2D QPI dispersion above the HOT[9] (see Sec. IV). $b^\dagger_{\mathbf{r}}, b_{\mathbf{r}}$ are slave-boson operators, introduced to account for fluctuations between singly and doubly occupied f-electron sites. Due to the particle-hole transformation discussed above, the constraint describing these fluctuations[12,13] is given by $\sum_\alpha f^\dagger_{\mathbf{r},\alpha} f_{\mathbf{r},\alpha} - b^\dagger_{\mathbf{r}} b_{\mathbf{r}} = 1$. Moreover, $I_{\mathbf{r},\mathbf{r}'}$ is the antiferromagnetic interaction between magnetic moments in the f-band, described by the $S = 1/2$ spin operator $\mathbf{S}^K_{\mathbf{r}}$ at site $\mathbf{r}$ (the origin of $I_{\mathbf{r},\mathbf{r}'}$ is discussed in Sec. IV).

In a path integral approach, one represents $\mathbf{S}^K_{\mathbf{r}}$ via the fermionic operators $f^\dagger, f$[14,15,17]; decouples the magnetic interaction term using a Hubbard-Stratonovich field, $\chi(\mathbf{r}, \mathbf{r}', \tau)$; and enforces the constraint by means of a Lagrange multiplier $(\epsilon_f - E_0)$. In the static (mean-field) approximation (and in the radial gauge[12,13]) one replaces $b^\dagger_{\mathbf{r}}, b_{\mathbf{r}}$ by their expectation value $\langle b^\dagger_{\mathbf{r}} \rangle = r_0(\mathbf{r}) e^{i\phi(\mathbf{r})}$ and subsumes the phase factor $e^{i\phi}$ into a redefinition of the fermionic-operators $f^\dagger, f$. A condensation of the bosonic

operators (i.e., $r_0 \neq 0$) represents the screening of the magnetic moments. One also replaces the field $\chi(\mathbf{r},\mathbf{r}',\tau)$ by its static expectation value $\chi(\mathbf{r},\mathbf{r}')$ which describes the antiferromagnetic correlations[18] between magnetic moments. Minimizing the effective action, we obtain the following set of self-consistent equations

$$\begin{aligned} s(\mathbf{r}) &= -\frac{J_0}{\pi}\int_{-\infty}^{\infty} d\omega\ n_F(\omega)\ \mathrm{Im}G_{fc}(\mathbf{r},\mathbf{r},\omega)\ ; \\ \chi(\mathbf{r},\mathbf{r}') &= -\frac{I_{\mathbf{r},\mathbf{r}'}}{\pi}\int_{-\infty}^{\infty} d\omega\ n_F(\omega)\ \mathrm{Im}G_{ff}(\mathbf{r},\mathbf{r}',\omega)\ ; \\ n_f(\mathbf{r}) &= -\int_{-\infty}^{\infty}\frac{d\omega}{\pi}\ n_F(\omega)\ \mathrm{Im}G_{ff}(\mathbf{r},\mathbf{r},\omega)\ , \end{aligned} \tag{2}$$

where $n_f(\mathbf{r}) = 1+r_0^2(\mathbf{r})$ and $J_0 = V^2/(\varepsilon_f - E_0) > 0$. The effective hybridization $s(\mathbf{r}) = Vr_0(\mathbf{r})$ is a measure for the screening of the magnetic moments. For a translationally invariant system, $s(\mathbf{r}) = s$ and $\chi(\mathbf{r},\mathbf{r}') = \chi_0$ and χ_1 for nearest and next-nearest-neighbor sites, respectively. This yields a dispersion of the heavy f-band given by

$$\chi_{\mathbf{k}} = -2\chi_0(\cos k_x + \cos k_y) - 4\chi_1 \cos k_x \cos k_y + \varepsilon_f\ . \tag{3}$$

Moreover, in this mean-field approximation, the full Green's functions ($\gamma,\zeta = c,f$)

$$G_{\gamma\zeta}(\mathbf{r}',\mathbf{r},\alpha,\tau) = -\langle T_\tau \gamma_{\mathbf{r}',\alpha}(\tau)\zeta^\dagger_{\mathbf{r},\alpha}(0)\rangle \tag{4}$$

describing the hybridization of the c- and f-electron bands are given by

$$\begin{aligned} G_{ff}(\mathbf{k},\alpha,\omega) &= \left[(G^0_{ff}(\mathbf{k},\alpha,\omega))^{-1} - s^2 G^0_{cc}(\mathbf{k},\alpha,\omega)\right]^{-1}\ ; \\ G_{cc}(\mathbf{k},\alpha,\omega) &= \left[(G^0_{cc}(\mathbf{k},\alpha,\omega))^{-1} - s^2 G^0_{ff}(\mathbf{k},\alpha,\omega)\right]^{-1}\ ; \\ G_{cf}(\mathbf{k},\alpha,\omega) &= -G^0_{cc}(\mathbf{k},\alpha,\omega) s G_{ff}(\mathbf{k},\alpha,\omega)\ , \end{aligned} \tag{5}$$

where $G^0_{ff} = (\omega + i\Gamma_f - \chi_{\mathbf{k}})^{-1}$, $G^0_{cc} = (\omega + i\Gamma_c - \varepsilon_{\mathbf{k}})^{-1}$, and Γ_c^{-1} and Γ_f^{-1} are the lifetimes of the c- and f-electron states, respectively (the potential origin of $\Gamma_{f,c}$ will be discussed below). For $\Gamma_c = \Gamma_f = 0^+$, the poles of the above Green's functions yield two energy bands with dispersion

$$E^{\pm}_{\mathbf{k}} = \frac{\varepsilon_{\mathbf{k}} + \chi_{\mathbf{k}}}{2} \pm \sqrt{\left(\frac{\varepsilon_{\mathbf{k}} - \chi_{\mathbf{k}}}{2}\right)^2 + s^2}\ . \tag{6}$$

To compute the differential conductance, dI/dV[19–21], measured in STS experiments[9,10], we define the spinor $\Psi^\dagger_{\mathbf{k},\alpha} = (c^\dagger_{\mathbf{k},\alpha}, f^\dagger_{\mathbf{k},\alpha})$ and the Green's function matrix $\hat{G}_\alpha(\mathbf{k},\tau) = -\langle T_\tau \Psi_{\mathbf{k},\alpha}(\tau)\Psi^\dagger_{\mathbf{k},\alpha}(0)\rangle$. With t_c and $t_f = t_f^{(0)} r_0$ being the tunneling amplitudes into the c- and f-electron bands, respectively, one has[20]

$$\frac{dI(\mathbf{r},\omega)}{dV} = -\frac{e}{\hbar}\hat{N}_t \sum_\alpha \sum_{i,j=1}^{2}\left[\hat{t}\,\mathrm{Im}\hat{G}_\alpha(\mathbf{r},\mathbf{r},\omega)\,\hat{t}\right]_{ij} \tag{7}$$

where $\hat{t} = \begin{pmatrix} t_c & 0 \\ 0 & t_f \end{pmatrix}$, and N_t is the STS tip's density of states, which is taken to be constant.

Finally, in the presence of impurities, dI/dV varies spatially, and the QPI spectrum, $S(\mathbf{q},\omega)$, is given by the Fourier transform of dI/dV into $\mathbf{q}$-space. In the Born approximation, we obtain

$$\begin{aligned} S(\mathbf{q},\omega) &\equiv \frac{dI(\mathbf{q},\omega)}{dV} = \frac{\pi e}{\hbar} N_t \sum_\alpha \sum_{i,j=1}^{2}\left[\hat{t}\hat{N}_\alpha(\mathbf{q},\omega)\hat{t}\right]_{ij}\ ; \\ \hat{N}_\alpha(\mathbf{q},\omega) &= -\frac{1}{\pi}\,\mathrm{Im}\int\frac{d^2k}{(2\pi)^2}\hat{G}_\alpha(\mathbf{k},\omega)\hat{U}\hat{G}_\alpha(\mathbf{k}+\mathbf{q},\omega), \end{aligned} \tag{8}$$

where

$$\hat{U} = \begin{pmatrix} U_c & U_{cf} \\ U_{fc} & U_f \end{pmatrix}\ . \tag{9}$$

Here, U_c and $U_f = U_f^{(0)} r_0^2$ are the Th-atoms'[9] scattering potential for intraband scattering in the c- and f-electron bands, respectively, while $U_{fc} = U_{cf} = U_{cf}^{(0)} r_0$ is the scattering potential for interband scattering between the c- and f-electron bands. We will show below that the experimental QPI spectrum provides insight into the relative strength of these scattering potentials. Finally, we note that $t_f^{(0)}$, $U_f^{(0)}$ and $U_{cf}^{(0)}$ are the tunneling amplitude and scattering strengths for the physical f-electron band, respectively[12,13].

III. RESULTS BELOW THE HOT

We begin by discussing the STS results of Schmidt *et al.*[9] obtained on a U-terminated surface of a 1% Th-doped sample. In Fig. 1(a) we present the experimental change in dI/dV below the HOT [$T = 1.9$K data of Fig. 3(b) in Ref.[9]] together with a theoretical fit, $\delta(dI/dV) = dI/dV(T < T_0) - dI/dV(T = T_0)$ (with $r_0 = 0$ at $T = T_0$) obtained from Eq.(7). In Figs. 1(c) and (d), we show a contour plot of the QPI intensity $|S(\mathbf{q},\omega)|$ (obtained with $U_f/U_c \approx 0.6$ and $U_{cf} = 0$) and the experimental QPI dispersions (black lines) of Figs. 5(c) and (d) in Ref.[9], along $q_y = 0$ and $q_y = q_x$ respectively. Figs. 1(e) and (f) show the maxima in $|S(\mathbf{q},\omega)|$, i.e., the QPI dispersion. The very good quantitative agreement between the theoretical and experimental dI/dV lineshapes and QPI dispersions suggests that the STS data reflect the emergence of a coherent Anderson lattice below the HOT, in agreement with the conclusions reached by Schmidt *et al.*[9]

We next discuss the QPI and dI/dV results in more detail. The QPI pattern is determined by scattering of electrons both within and between the $E^{\pm}_{\mathbf{k}}$-bands. Intraband scattering [see Fig. 1(b)] gives rise to the $\mathbf{q}_1$ and $\mathbf{q}_2$ branches in $|S(\mathbf{q},\omega)|$ shown in Figs. 1(c) and (d). The main contribution to these branches arises from $2k_F$-scattering [Fig. 1(b)], such that their dispersion is

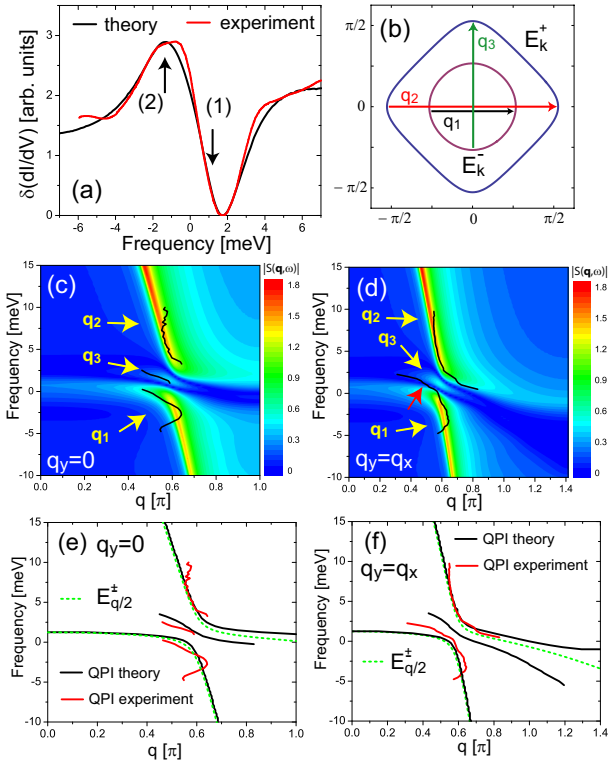

FIG. 1. (color online) (a) Experimental[9] and theoretical $\delta(dI/dV)$ below the HOT. A background was subtracted and the data were vertically scaled. (b) Fermi surfaces of $E^{\pm}_{\mathbf{k}}$. Contour plot of $|S(\mathbf{q},\omega)|$ along (c) $q_y = 0$ and (d) $q_y = q_x$, together with the QPI dispersions of Ref.[9]. (e),(f) Maxima of $|S(\mathbf{q},\omega)|$. The theoretical parameters are $t = 45$ meV, $\mu = 3.17t$, $s = 0.06t$, $\varepsilon_f = -0.08t$, $\chi_0 = -0.04t$, $\chi_1 = -0.3\chi_0$, $t_f/t_c = 0.0075$, $U_f/U_c = 0.6$, $\Gamma_{f,c} = 0.03t$, yielding $r_0^2 = 0.51$, $V = 0.084t$, $E_0 = -0.082t$, $J_0 = 2.95t$, and $I = 0.42t$.

approximately described by $E^{\pm}_{\mathbf{q/2}}$ as shown in Figs. 1(e) and (f). Moreover, $E^{\pm}_{\mathbf{k}}$ overlap in the energy interval -1 meV $\lesssim \omega \lesssim 1.5$ meV, thus allowing for interband scattering with wave-vector $\mathbf{q}_3$, and a corresponding $\mathbf{q}_3$ branch in $|S(\mathbf{q},\omega)|$ [see Figs. 1(c) and (d)]. The $\mathbf{q}_3$ branch has been seen experimentally along $q_y = 0$, where the experimental and theoretical QPI results are in very good agreement, but is absent along $q_y = q_x$. The latter discrepancy likely arises from the smaller gap along $q_y = q_x$ rendering the experimental resolution of the $\mathbf{q}_1$ and $\mathbf{q}_3$ branches difficult. As a result, the experimental $\mathbf{q}_1$ branch around $q \approx 0.5\pi$ lies between the theoretical $\mathbf{q}_1$ and $\mathbf{q}_3$ branches [see red arrow in Fig. 1(d)]. This difficulty in resolving the two branches also explains why the extrapolation of the $\mathbf{q}_1$ dispersion to $q = 0$ along $q_y = 0$ yields an energy of $\omega \approx 1$ meV for the upper band edge of $E^-_{\mathbf{k}}$ which is consistent with the sharp drop in dI/dV at this energy [see arrow (1) in Fig. 1(a)], while the extrapolation along $q_y = q_x$ does not. Moreover, the good agreement between the theoretical and experimental QPI dispersions also allows us to identify the peak in dI/dV at $\omega = -2$ meV [see arrow (2) in Fig. 1(a)] as arising from the van Hove singularity of the f-electron band.

The experimental QPI data[9] also provide insight into the microscopic nature of Th-scattering, since the QPI dispersion, as well as the spectral weight associated with the QPI spectrum $|S(\mathbf{q},\omega)|$ sensitively depend on the relative strength of the scattering potentials. To demonstrate this, we present in Fig. 2(a) the QPI spectrum for intraband scattering in the c-band only, i.e., for $U_f, U_{cf} = 0$, $U_c \neq 0$. This spectrum is similar to that

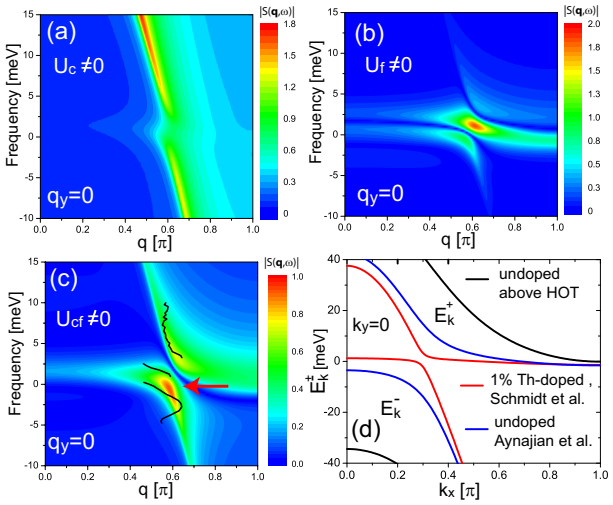

FIG. 2. (color online) $|S(\mathbf{q},\omega)|$ along $q_y = 0$ for (a) $U_f, U_{cf} = 0$, $U_c \neq 0$, (b) $U_c, U_{cf} = 0$, $U_f \neq 0$, and (c) $U_f, U_c = 0$, $U_{cf} \neq 0$. (d) $E^{\pm}_{\mathbf{k}}$ extracted from theoretical fits.

of the unhybridized c-electron band [see Fig. 4(a)] since its dominant contribution arises from scattering between states where the coherence factors of the c-electrons are large. Conversely, for intraband scattering in the f-band, i.e., for $U_c, U_{cf} = 0$, $U_f \neq 0$, the QPI spectrum $|S(\mathbf{q},\omega)|$ shown in Fig. 2(b) is predominantly determined by scattering between states with large f-electron weight. The spectral weight in $|S(\mathbf{q},\omega)|$ in both cases [Figs. 2(a) and (b)] is inconsistent with the experimentally observed QPI weight and dispersion. The latter can only be explained (as shown in Fig. 1) by considering intraband scattering both in the c- and f-bands with relative scattering strength $U_f/U_c \approx 0.6$. Finally, for interband scattering between the c and f-bands, i.e., for $U_f, U_c = 0$, $U_{cf} \neq 0$, the QPI spectrum significantly deviates from the experimental QPI dispersion, as shown in Fig. 2(c). In particular, interband scattering leads to only two branches in the QPI spectrum, in contrast to the three branches observed experimentally. Moreover, the largest spectral weight in the QPI spectrum for interband scattering occurs where the experimental QPI intensity is close to a minimum [see red arrow in Fig. 2(c)]. Note in this regard that the existence of a $\mathbf{q}_3$ branch from interband scattering between the $E^{\pm}_{\mathbf{k}}$-bands [see Fig. 1(b)] does not require $U_{cf} \neq 0$. These inconsistencies thus strongly suggest that Th-atoms do not lead to interband scattering

between the c and f-bands.

We next discuss the STS results by Aynajian *et al.*[10], and present in Figs. 3(a) and (b) the experimental dI/dV data obtained on a U-terminated surface of pure URu_2Si_2 for $T = 2$K and 4K, respectively [Fig. 4(b) in Ref.[10]], together with the theoretical results obtained from Eq.(7). The theoretical dI/dV curves reproduce the experiment's salient features: the asymmetry and magnitude of the gap in dI/dV as well as the peak at $\omega \approx -0.8$ meV [see arrows in Figs. 3(a) and (b)] which arises from the van Hove singularity of the f-electron band. (similar results were recently reported for $YbRh_2Si_2$[22], and the Si-terminated surface of URu_2Si_2[9]). Both features are

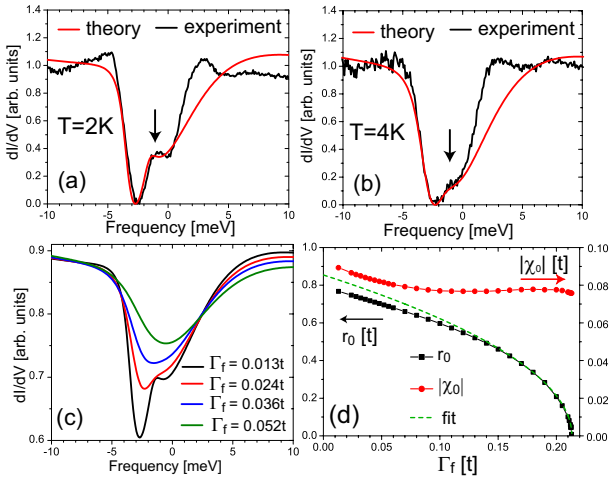

FIG. 3. (color online) Theoretical fits to the dI/dV data of Ref.[10] at (a) $T = 2$K and (b) $T = 4$K. (c) Evolution of dI/dV with Γ_f. The theoretical parameters are $J = 3.69t$, $I = 0.89t$, $\chi_1 = -0.36\chi_0$, $t_f/t_c = 0.0175$, and $\Gamma_c = 0.02t$. At $T = 2$K, $s = 0.32t$ $\varepsilon_f = -0.20t$, $\chi_0 = -0.09t$, $V = 0.418t$, $E_0 = -0.25t$. (d) Dependence of r_0 and $|\chi_0|$ on Γ_f. The green line is a fit to $r_0 = 0.765t(\Gamma_f^0 - \Gamma_f)^{0.5}$ with $\Gamma_f^0 = 0.21315t$.

characteristic signatures of the Anderson lattice bandstructure, and thus suggest the existence of a coherent Anderson lattice below the HOT.

To gain insight into the microscopic origin of the CAL, we note that the changes in dI/dV between $T = 2$K [Fig. 3(a)] and $T = 4$K [Fig. 3(b)] can be solely attributed to an increase in the damping of the f-electron states from $\Gamma_f = 0.013t$ at $T = 2$K to $\Gamma_f = 0.024t$ at $T = 4$K, and the concomitant reduction in the magnitude of r_0, χ_0 [see Fig. 3(d)], and ε_f obtained from the self-consistent solution of Eq.(2) (a more detailed discussion of this procedure is given below). Increasing Γ_f even further yields the evolution of dI/dV shown in Fig. 3(c) which possesses the same characteristic signatures as those observed by Aynajian *et al.*[10] with increasing temperature: the gap in dI/dV is filled in, its magnitude remains approximately constant (until close to the HOT), and the center of the gap shifts to larger energies. We therefore conclude that the formation of a coherent Anderson lattice below the HOT is likely driven by a significant reduction of Γ_f with decreasing temperature. In Fig. 3(d) we present the corresponding evolution of r_0 and χ_0 with Γ_f [obtained from Eq.(2)] that enters the calculation of dI/dV shown in Fig. 3(c). While r_0 decreases only by approximately 10% between $\Gamma_f = 0.013t$ and $0.052t$, it is the interplay between this decrease in r_0 and the increase in Γ_f that leads to the substantial evolution of the dI/dV curves in Fig. 3(c). With increasing Γ_f, r_0 decreases monotonically and vanishes at $\Gamma_f^0 = 0.21315t$, varying as $r_0 \approx 0.765t(\Gamma_f^0 - \Gamma_f)^{1/2}$ for $\Gamma_f \lesssim \Gamma_f^0$ [see dashed green line in Fig. 3(d)].

In Fig. 2(d), we present the bandstructure, $E_{\mathbf{k}}^{\pm}$, resulting from our fits for 1% Th-doped[9] (Figs. 1) and pure URu_2Si_2[10] (Figs. 3) samples. In the Th-doped sample, the hybridization is smaller while $\Gamma_{f,c}$ are larger than in the undoped compound. These results are consistent with a suppression of the HOT (and thus s) and an increased decoherence by Th-doping (however, the microscopic origin for the experimentally observed strong suppression of the hybridization by 1% Th-doping is currently unclear). This, together with the similar extracted f-electron densities of $n_f = 1.59$ in the pure and $n_f = 1.51$ in the Th-doped samples, supports the conclusions that both groups probe the same heavy and light bands, and that URu_2Si_2 represents a coherent Anderson lattice system below the HOT.

We next discuss the parameters extracted from our analysis of the experimental data, as well as the self-consistent solution of Eq.(2) in more detail. We find that the theoretical fits shown in Figs. 1 and 3(a) for 1% Th-doped[9] and pure URu_2Si_2[10], and the parameters (i.e., s, ε_f, $\chi_{0,1}$, t_f/t_c, U_f/U_c, $\Gamma_{f,c}$) extracted from these fits are unique since each theoretical parameter exerts a qualitatively different effect on the dI/dV and QPI spectra, as discussed in Ref.[20] and shown above for U_f/U_c [we note here that the c-band dispersion, $\varepsilon_{\mathbf{k}}$, is uniquely determined by the QPI spectrum above the HOT, see Fig. 4(a)]. When one considers the evolution of dI/dV with increasing Γ_f, as we did in Fig. 3, the question immediately arises of which parameters remain unaffected by the changing Γ_f. In addition to the magnetic interaction I, one might assume that the bare hybridization, V, which is computed via $V = s/r_0$ and $r_0 = \sqrt{n_f - 1}$, where n_f is obtained from Eq.(2), as well as E_0 will remain unchanged. However, both V and E_0 are computed using n_f, whose uncertainty could be substantial since it is predominantly determined by regions of the BZ where no experimental QPI data are available to test the accuracy of our theoretical fits. In particular, due to the large mass of the f-dispersion, $\chi_{\mathbf{k}}$, small changes in band parameters (or further magnetic interactions) could significantly alter n_f (and hence V and E_0), for example, through the existence of additional Fermi surface pockets[8]. Moreover, the physical mechanism changing Γ_f (with increasing temperature) could also affect E_0 due to the its proximity to the Fermi energy. In order to avoid these uncertainties in the self-consistent solution of Eq.(2), we therefore assumed that J_0 (and I) remain un-

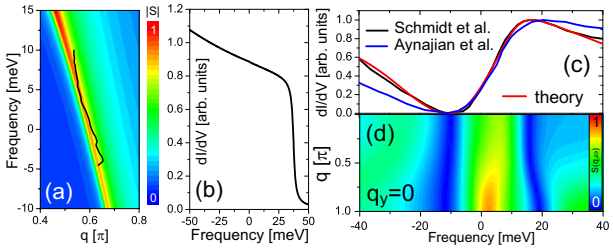

FIG. 4. (color online) Above the HOT: (a) $|S(\mathbf{q},\omega)|$ for $q_x = q_y$ together with the experimental QPI dispersion of Ref.[9], and (b) dI/dV, both for the same parameters as in Fig. 1 but $s = 0$. (c) Theoretical fit to the 19K dI/dV data [Fig.5(c) in Ref.[9]] with $s = 1.0t$, $\chi_0 = -0.045t$, $\chi_1 = 0$, $\varepsilon_f = -0.032t$, $\Gamma_c = 0.77t$, $\Gamma_f = 0.13t$, and (d) the resulting $|S(\mathbf{q},\omega)|$ along $q_y = 0$.

changed with increasing Γ_f, resulting in the good agreement of our theoretical dI/dV curves [Figs. 3(b) and (c)] with the experimental data.

The above results also provide insight into the origin of the magnetic interaction, $I_{\mathbf{r},\mathbf{r}'}$, which can arise from direct exchange[23,24] or from an RKKY interaction[3,16,25]. While our analysis has shown that $I_{\mathbf{r},\mathbf{r}'}$ between nearest-neighbor sites is antiferromagnetic, we find that the RKKY-interaction between nearest neighbor sites (which we computed using the extracted bandstructure) is ferromagnetic. This result suggests that the microscopic origin of the nearest-neighbor $I_{\mathbf{r},\mathbf{r}'}$ in URu_2Si_2 lies in direct exchange, and not in an RKKY interaction.

Finally, our good theoretical fits of the experimental STS results in terms of a coherent Anderson lattice suggest that the STS data exhibit no signature (within the accuracy of the theoretical fit) of a hidden order parameter (though it was recently argued that the HOP might be "hidden" in the hybridization[26]). While the microscopic origin of a finite $\Gamma_{f,c}$ is presently unclear and might lie in the presence of disorder or the coupling to collective modes, the drastic decrease in Γ_f below the HOT could be an indirect signature of the emergence of the hidden order parameter, if the latter were to suppress those fluctuation channels that are the physical origin of a non-zero Γ_f.

IV. RESULTS ABOVE THE HOT

We next discuss the dI/dV Fano-lineshape observed above the HOT[9,10] and its relation to the conduction band observed in QPI[9]. The QPI intensity, $|S(\mathbf{q},\omega)|$, for $T > T_0$ where $r_0 = 0$, shown in Fig. 4(a) reproduces well the experimental QPI dispersion (black line) of Fig. 5(b) in Ref.[9]. The dI/dV lineshape resulting from this light band does not exhibit the characteristic Fano form (the sharp drop in dI/dV at $\omega \approx 40$meV signifies the upper band edge of $\varepsilon_{\mathbf{k}}$), implying that the origin of the latter lies in electronic bands not yet seen in QPI. This conclusion is also supported by a theoretical fit of the experimental dI/dV data of Ref.[9] and Ref.[10] above the HOT, shown in Fig. 4(c). The resulting bands, $E^{\pm}_{\mathbf{k}}$, shown in Fig. 2(d) (black lines), are not only significantly different from the ones seen in QPI below the HOT, but also exhibit much larger quasi-particle dampings, $\Gamma_{f,c}$, thus representing an *incoherent Anderson lattice*. As a result, $|S(\mathbf{q},\omega)|$, shown in Fig. 4(d), exhibits very little $\mathbf{q}$-structure (for fixed ω), thus explaining the difficulty in detecting these bands in QPI. We therefore conclude that an explanation of the STS data above and below the HOT likely requires multiple sets of c- and f-electron bands.

V. CONCLUSIONS

In summary, we have shown that recent STS results[9,10] are consistent with the presence of a coherent Anderson lattice in URu_2Si_2 below the HOT, but show no direct signature of the hidden order parameter. We argue that the emergence of the CAL is driven by a drastic increase in the quasi-particle coherence, which could be an indirect signature of the hidden order parameter. Clearly, further studies are required to investigate this possibility.

Acknowledgements

We would like to thank P. Aynajian, J.C. Davis, and A. Yazdani for stimulating discussions and comments, and for providing us with their experimental data. This work is supported by the U.S. Department of Energy under Award No. DE-FG02-05ER46225.

[1] M.B. Maple *et al.*, J. Low Temp. Phys. **99**, 223 (1995); A. Schroder *et al.* Nature (London) **407**, 351 (2000); G.R. Stewart, Rev. Mod. Phys. **73**, 797 (2001); J. Custers, *et al.* Nature (London) **424**, 524 (2003); H. von Lohneysen *et al.*, Rev. Mod. Phys. **79**, 1015 (2007); P. Gegenwart, Q. Si, and F. Steglich, Nature Physics, **4**, 186 (2008).
[2] J. Kondo, Prog. Theor. Phys. **32**, 37 (1964).
[3] S. Doniach, Physica B **91**, 231 (1977).
[4] T. T. M. Palstra *et al.* Phys. Rev. Lett. **55** 2727 (1985).
[5] M.B. Maple, *et al.* Phys. Rev. Lett. **56**, 185 (1986).

[6] J. Schoenes *et al.*, Phys. Rev. B **35**, 5375 (1987); D.A. Bonn *et al.*, Phys. Rev. Lett. **61**, 1305 (1988); S.V. Dordevic, *et al.*, Phys. Rev. Lett. **86**, 684 (2001); J.G. Rodrigo *et al.* Phys. Rev. B. **55**, 14318 (1997); R. Escudero, F. Morales, and P. Lejay, Phys. Rev. B **49**, 15271 (1994); J.D. Denlinger *et al.*, J. Elec. Spectrosc. **117118**, 347 (2001).

[7] D.L. Cox, Phys Rev Lett **59**, 1240 (1987); P. Chandra *et al.*, Nature **417**, 831 (2002); C.M. Varma and L. Zhu, Phys. Rev. Lett. **96**, 036405 (2006); A.V. Balatsky *et al.*, Phys. Rev. B **79**, 214413 (2009); S. Elgazzar, *et al.*, Nature Mater. **8**, 337 (2009); C. Pepin *et al.*, arXiv:1010.1237; Y. Dubi and A.V. Balatsky, arxiv:1011.5315.

[8] K. Haule, and G. Kotliar, Nature Phys. **5**, 796 (2009); P. M. Oppeneer *et al.*, Phys. Rev. B **82**, 205103 (2010).

[9] A.R. Schmidt *et al. Nature* **465**, 570 (2010).

[10] P. Aynajian *et al.*, PNAS **107**, 10383 (2010).

[11] U. Fano, Phys. Rev. **124**, 1866 (1961).

[12] P. Coleman, Phys. Rev. B **29**, 3035 (1984).

[13] A.J. Millis and P.A. Lee, Phys. Rev. B **35**, 3394 (1987); D.M. Newns and N. Read, Adv. Phys. **36**, 799 (1987).

[14] G. Kotliar and J. Liu, Phys. Rev. B **38**, 5142 (1988)

[15] A. D. Hewson, *The Kondo Problem to Heavy Fermions* (Cambridge University Press, Cambridge, 1997).

[16] P. Coleman, *Handbook of Magnetism and Advanced Magnetic Materials* (Wiley and Sons, 2007).

[17] N. Read and D. M. Newns, J. Phys. C **16**, 3273 (1983); P. Coleman, Phys. Rev. B **28**, 5255 (1983); N. E. Bickers, Rev. Mod. Phys. **59**, 845 (1987).

[18] T. Senthil, S. Sachdev, and M. Vojta, Phys. Rev. Lett. **90**, 216403 (2003); I. Paul, C. Pepin, and M.R. Norman, Phys. Rev. Lett. **98**, 026402 (2007), J.Figgins and D.K. Morr, Phys. Rev. Lett. **107**, 066401 (2011).

[19] M. Maltseva, M. Dzero, and P. Coleman, Phys. Rev. Lett. **103**, 206402 (2009).

[20] J. Figgins, and D.K. Morr, Phys. Rev. Lett. **104**, 187202 (2010).

[21] P. Wölfle, Y. Dubi, and A.V. Balatsky, Phys. Rev. Lett. **105**, 246401 (2010).

[22] S. Ernst *et al.*, Nature **474**, 362 (2011).

[23] T. Senthil, S. Sachdev, and M. Vojta, Phys. Rev. Lett. **90**, 216403 (2003).

[24] I. Paul, C. Pepin, and M.R. Norman, Phys. Rev. Lett. **98**, 026402 (2007).

[25] Q.M. Si *et al.*, Nature **413**, 804 (2001).

[26] P. Chandra, P. Coleman, and R. Flint, preprint.